Self-healing capacity of Mullite-Yb_2SiO_5 environmental barrier coating material with embedded Ti_2AlC MAX phase particles

Lee, Gye Won; Kim, Tae Woo; Sloof, Willem G.; Lee, Kee Sung

DOI
10.1016/j.ceramint.2021.04.257

Publication date
2021

Document Version
Accepted author manuscript

Published in
Ceramics International

Ceramics International xxx (xxxx) 1–9

Contents lists available at ScienceDirect

Ceramics International

journal homepage: www.elsevier.com/locate/ceramint

Self-healing capacity of Mullite-Yb_2SiO_5 environmental barrier coating material with embedded Ti_2AlC MAX phase particles

Gye Won Lee [a], Tae Woo Kim [a], Willem G. Sloof [b], Kee Sung Lee [a, *]

[a] School of Mechanical Engineering, Kookmin University, Seoul 02707, South Korea
[b] Department of Materials Science and Engineering, Delft University of Technology, Mekelweg 2, 2628 CD Delft, the Netherlands

ARTICLE INFO

Keywords:
Environmental barrier coating
Crack healing
Ti_2AlC
Mechanical properties

ABSTRACT

Repetitive heating and cooling cycles inevitably cause crack damage of hot gas components of gas turbine engines, such as blades and vanes. In this study the self-healing capacity is investigated of mullite + ytterbium monosilicate (Yb_2SiO_5) as EBC material with Ti_2AlC MAX phase particles embedded as a crack-healing agent. The effect of Ti_2AlC in the EBC was compared with the self-healing ability of the mullite + Yb_2SiO_5 material. After introducing cracks by Vickers indentation on the surface of each sample, crack healing was realized by controlling the temperature and time during the post-heat-treatment process. For the mullite + Yb_2SiO_5 composite with Ti_2AlC particles, crack healing occurred at 1000 °C, while in the case of the mullite + Yb_2SiO_5 composite without Ti_2AlC, a sustained temperature of 1300 °C or higher was required. Compared with the healing of the mullite + Yb_2SiO_5 composite by the formation of a eutectic phase, the addition of Ti_2AlC promoted healing via the oxidation of Ti and Al. Notably, the surface formation of a ternary oxide of Ti–Yb–O was confirmed, which completely covered the damage area. Consequently, the addition of a Ti_2AlC MAX phase to the EBC composite resulted in a complete strength recovery, while the mullite + Yb_2SiO_5 composite without Ti_2AlC showed a strength recovery of about 80%. Furthermore, by analyzing the indentation load–displacement curve to indicate the role of Ti_2AlC, the addition of Ti_2AlC improved both the hardness and stiffness of the composite.

1. Introduction

Ceramic thermal barrier coatings (TBC) have been developed and applied to offer thermal protection and enhance the operation efficiency of gas turbine systems for power and propulsion generation in aerospace industries [1–5]. More recently, to meet the demand for increasing the gas turbine operation temperature, attempts have been made to replace heat-resistant alloys in hot gas components with those prepared from all-ceramic composites [6]. One of the most promising materials is silicon carbide (SiC) composite reinforced with SiC fibers. These SiC–SiC composites have excellent heat-resistant and mechanical properties and remain robust even at operating temperatures above those at which heat-resistant alloys can be used [7].

However, a disadvantage of SiC–SiC composites is that at high temperatures, mass reduction occurs during reaction with water vapor as a consequence of combustion. In a high temperature combustion environment, reaction between SiC and water vapor results in volatile $Si(OH)_4$, leading to a high mass recession rate [8]. The SiC–SiC composite can be protected by applying an environmental barrier coating (EBC) on the surface to mitigate the problem of mass loss due to such high-temperature corrosion [6,9–15]. Oxides such as mullite and ZrO_2 have been studied [16–18] as potential EBC topcoat material, while more recently, rare-earth-based oxides have received a lot of attention [12,13,15,19–23]. As a representative material, Ytterbium (Yb)-based silicate oxide is believed to possess excellent durability under high-temperature water vapor conditions.

When a TBC or EBC is applied to the hot gas parts of turbine components, an environment is encountered that is repeatedly exposed to a thermal shock condition due to the cooling from a high operating temperature to room temperature. As the coating material is adhered to the substrate, it is subjected to thermal stress, i.e., during the heat change process, thermal expansion and contraction remain in a constrained state. When the thermal stress is greater than the stress that the material can withstand, cracks inevitably occur in the relatively brittle coating material due to the difference in coefficient of thermal expansion between the coating and substrate. For example, vertical cracks in the

* Corresponding author.
E-mail address: keeslee@kookmin.ac.kr (K.S. Lee).

https://doi.org/10.1016/j.ceramint.2021.04.257
Received 28 December 2020; Received in revised form 22 April 2021; Accepted 26 April 2021
0272-8842/

Table 1
Basic characteristics of the materials before and after crack healing.

Material	Density (g/cm3)	Hardness[a] (kgf/mm2)		Relative elasticmodulus[b]	
		Before	After	Before	After
Mullite	2.23	552 ± 165	–	100%	–
Mullite + Yb2SiO5	2.80	1285 ± 242	931 ± 27[c]	141%	149%[c]
Mullite + Yb2SiO5 +Ti2AlC	4.09	1520 ± 118	1077 ± 225[d]	161%	151%[d]

[a] Data from Vickers indentation.
[b] Data from spherical indentation (see Fig. 10).
[c] After 1500 °C, 2hr, 1cycle.
[d] After 1000 °C, 2hr, 1cycle.

TBC topcoat and mud cracks in the EBC topcoat have both been reported [24–27]; analysis revealed that these cracks occurred after exposure to high temperatures. Vertical cracks are relatively stable; however, when the cracks grow along the interface layer between the coating and sublayer, interfacial delamination occurs, resulting in the eventual delamination of the coating layer and the loss of protection to the underlying material [28]. Therefore, turbine engines for power generation and propulsion in are regularly inspected for cracks and subsequently any damage is repaired.

The self-healing ability of a material to repair these cracks at high operating temperatures of a turbine engine is being studied [4,5,29]. Self-healing technology can significantly contribute to the improvement of the durability of turbine parts since any cracks formed in the coating layer are self-healed during heating to operating temperatures, even if they occur due to the difference in the thermal expansion coefficient during cooling. Implementation of self-healing technology, wherein cracks are self-healed at the operating temperature of a turbine, mitigate the crack damage and thereby extent the lifetime of critical hot gas components.

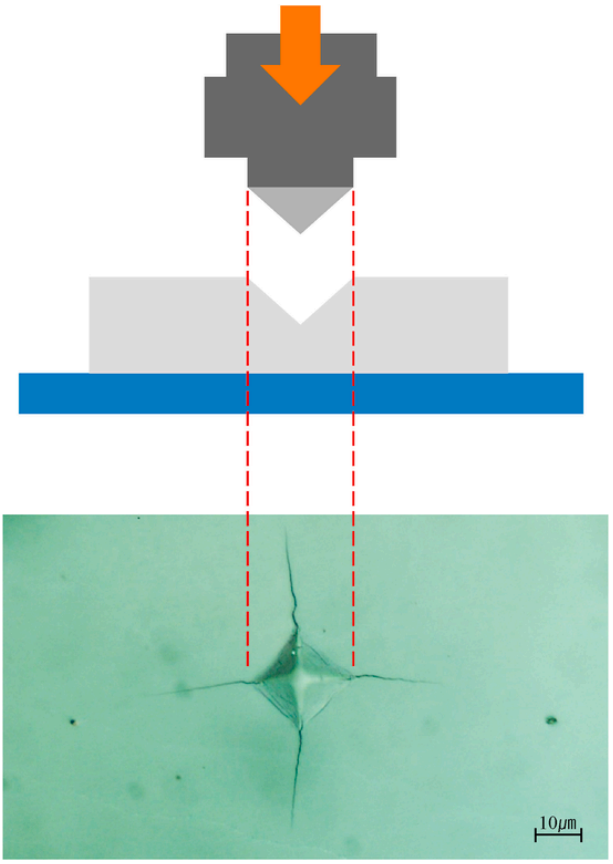

Fig. 1. Vickers indentation to create radial cracks in the ceramic composite samples.

Three types of crack-healing methods are related presently to ceramics, viz.: sintering, formation of liquid phase and oxidation of sacrificial embedded particles. In the first type of crack healing, sintering occurs of isolated crack-like pores [30]. In the second type of crack healing, the material's second phase (usually liquid phase at high temperature) fills the cracks and heals the damage [31]. In the third type of crack healing, oxides are formed by the oxidation of sacrificial particles or matrix material, i.e., either intrinsic or extrinsic, which expand into the cracks and heal the damage [32–34].

The previous studies have reported that SiC oxidizes to viscous SiO_2 at high temperatures, and the viscous phases fill and heal the cracks [31,35,36]. Recently, we reported a phenomenon in which a molten phase is formed by a eutectic reaction, and the cracks are healed when repeated thermal shock is applied to 5000 cycles at a temperature of 1350 °C in a mullite + Yb_2SiO_5 composite [37]. For high-temperature applications, studies into crack healing using MAX phase ceramics have also attracted attention [34,38,39]. These ceramics has demonstrated the ability to autonomously and intrinsically heal cracks by oxidation at high temperatures. The MAX phase is a ternary compound represented by $M_{n+1}AX_n$, where n = 1–3, M is a transition metal, A is A group element (mostly IIIA and IVA such as aluminum (Al) or silicon (Si)), and X is carbon (C) or nitrogen (N). This material is confirmed to be stable up to 1500 °C and has excellent thermal shock resistance [39]. As it possesses a layered ternary structure, its damage tolerance is outstanding and it is machinable [38,39]. Upon exposure of the MAX phases, such as Ti_2AlC or Ti_3AlC_2, to high temperatures in an oxidizing environment, preferentially A element oxide is formed which also exhibit a much faster diffusion rate than the M element. Due to volume expansion this oxide is filling the crack gaps and restore the component integrity [34,40–44].

Although cracks in SiC can be healed by the oxidation of SiC at high temperatures above a specific threshold, high-temperature corrosion is easily caused by the newly formed SiO_2 [9]. Crack healing has been reported in both mullite- and Yb-based EBC, but it is believed that healing occurs only after sustained exposure to extremely high temperatures of 1350 °C [37]. Hence, it is more attractive to investigate extrinsic crack healing induced by oxidation. In this study, self-healing of a mullite + Yb_2SiO_5 composite with embedded MAX phase particles is investigated. To this end, the flexural strength characteristics as well as the mechanical behavior, as obtained from indentation load–displacement curve using a spherical indenter, were determined before and after healing of cracks induced by Vickers indentation [22,25,38,45].

2. Experimental procedures

2.1. Preparation of EBC materials and MAX phase

First, Yb_2SiO_5 powder was synthesized to prepare the mullite + Yb_2SiO_5 composite. The starting powders of Yb_2O_3 (3 N, Kojundo Chemical Laboratory Co., Ltd, Saitama, Japan) and SiO_2 (Kojundo Chemical Laboratory Co., Ltd, Saitama, Japan) were mixed at a molar ratio of 1:1. Then, the powders were dispersed in an isopropanol in a polypropylene container and ball milled with zirconia balls for 24 h. After milling, the solvent of the powder was volatilized for 1–2 days, and after crushing the dried cake in a mortar, granulated powders were prepared using a 60 μm sieve. Thereafter, the powders were heat treated in air at 1400 °C for 20 h to synthesize the Yb_2SiO_5 powder.

The prepared Yb_2SiO_5 powder was mixed again with the mullite powder (DURAMUL, 325F, Washington Mills, NY, USA). The weight ratio of Yb_2SiO_5 was controlled within the range of 10–50 wt% for the entire batch. The same ball milling, drying, and sieving process was used to prepare the mullite + Yb_2SiO_5 mixed powder. The powder was

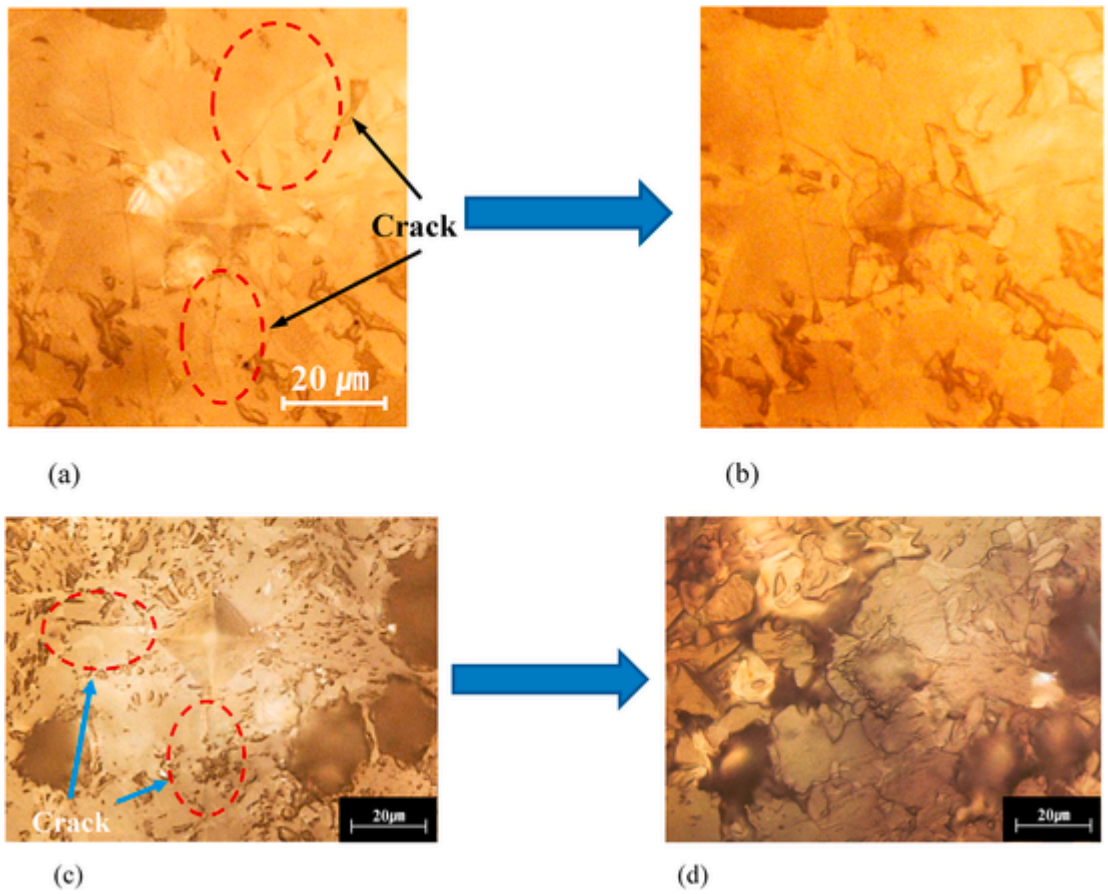

Fig. 2. Micrographs of Vickers radial cracks (P = 1.96 N) in the mullite + Yb_2SiO_5 composite: (a) crack area before and (b) after three cycles of heat treatment in air at 1350 °C for 10 h; and (c) crack area before and (d) after heat treatment in air at 1500 °C for 2 h. Note that the radial cracks virtually disappeared due to healing.

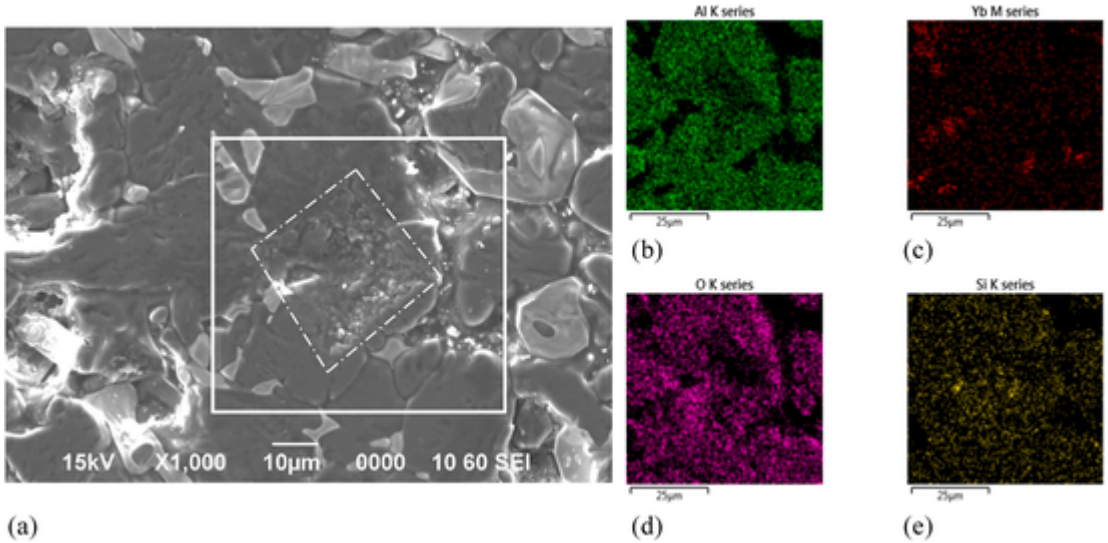

Fig. 3. Analysis results after crack healing at 1500 °C in the mullite + Yb_2SiO_5 composite. The composite was analyzed by (a) SEM and (b)~(e) XMA. The rectangular mark indicates the analysis area, and the dotted mark denotes the plastic damage caused by Vickers indentation.

pressed with a pressure of 50 MPa into a disc with a diameter of 25.4 mm or 30 mm width × 40 mm length using stainless mold (HMM-04A, Hansung Systems Inc., Korea) before being pressed with a cold isostatic press (SCIP-50/150, Samyang Ceratech. Co., Korea) at a pressure of 200 MPa. Finally, pressureless sintering was performed in air at 1500–1600 °C for 1–10 h with a heating rate of 5 °C/min.

For the MAX phase, titanium (Ti, 99%, 5 μm, US Research Nanomaterials Inc., USA), titanium carbide (TiC, 99.99%, 3 μm, Kojundo Chemical Laboratory Co., Japan), and aluminum powders (Al, 99.5%, 3 μm, Kojundo Chemical, Japan) were used. The Ti, Al, and TiC powders were mixed at a molar ratio combination. Zirconia balls were added in the same manner as in the Yb_2SiO_5 powder process, and wet

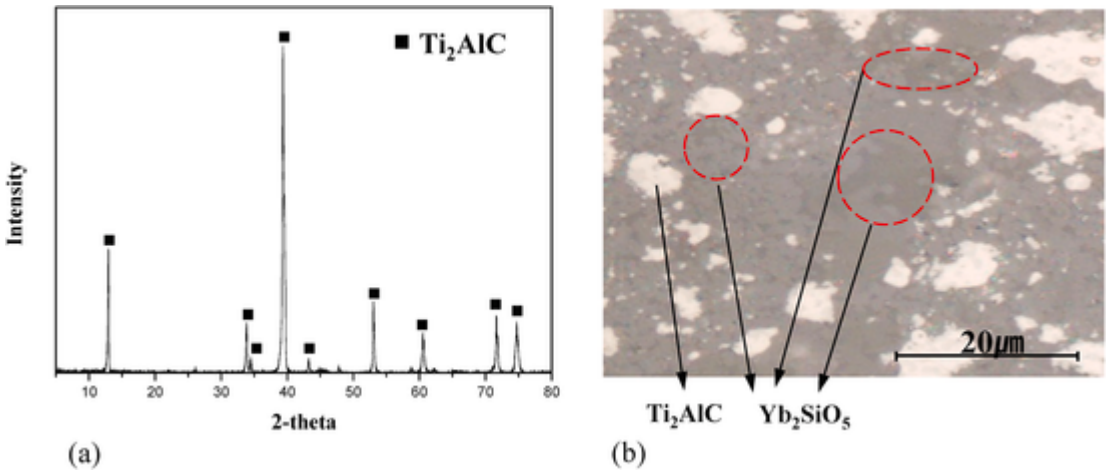

Fig. 4. Analysis of the mullite + Yb_2SiO_5 composite with Ti_2AlC embedded particles. (a) Diffractogram of the white phase in the micrograph, and (b) micrograph of the microstructure of the composite as observed with optical microscopy.

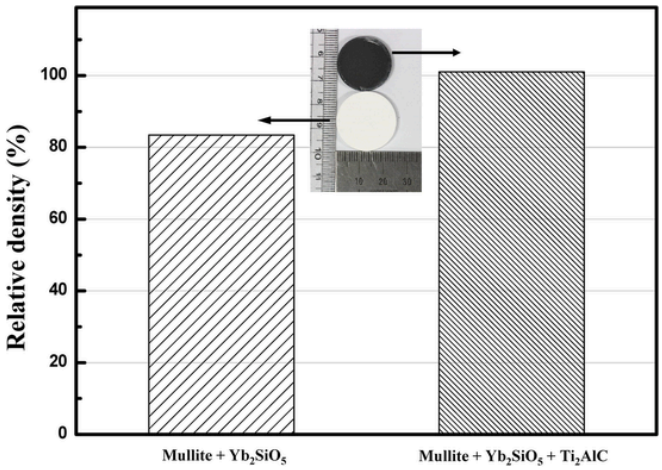

Fig. 5. Relative densities of mullite + Yb_2SiO_5 composite with and without Ti_2AlC embedded particles. Note the difference in diameter between the mullite + Yb_2SiO_5 with and without Ti_2AlC embedded particles. Both samples were prepared at the same sintering temperature.

ball milling was performed for 24 h using isopropanol as a lubricant. After this process was complete, drying was performed at room temperature before sieving through a 60 μm sieve. Ti_2AlC powder was synthesized by pressing and heat treating the sieved powder at 1350–1550 °C. The synthesized Ti_2AlC was pulverized with a tungsten carbide ball using a SPEX Mill (Taemyong Scientific Co. Ltd., Korea). Next, the powders were ball milled again using the same process as for the Yb_2SiO_5 powders, and wet ball milling was performed for 24 h using isopropanol. Then, the powders were sieved with a 60 μm sieve. Only the powder that passed through the sieve were used as healing agent.

Finally, the MAX-phase-added mullite + Yb_2SiO_5 composite for crack healing was prepared. Firstly, the mixed mullite + Yb_2SiO_5 powder was prepared as described above and subsequently mixed with the granulated Ti_2AlC powder at a weight ratio of approximately 8:2 before being dispersed in isopropanol. Secondly, wet ball milling was performed for 24 h using ZrO_2 balls in the same way as in the Ti_2AlC milling process. Then, the wet powders were dried at room temperature for 1–2 days. Finally, the mixed composite powders were obtained via sieving using a 60 μm sieve.

The Ti_2AlC-added mullite + Yb_2SiO_5 composites were uniaxially pressed at a pressure of 50 MPa using a mold with a diameter of 25.4 mm or 30 mm width × 40 mm length (HMM-04A, Hansung Systems Inc., Korea). Additionally, cold isostatic pressing (with SCIP-50/150, Samyang Ceratech. Co., Korea) was performed at a pressure of 200 MPa. Next, the pellets were sintered by heat treatment in air at 1400–1600 °C for 2 h with a heating rate of 5 °C/min.

2.2. Characterization

The densities of the mullite + Yb_2SiO_5 and Ti_2AlC-added mullite + Yb_2SiO_5 composites were measured adopting the Archimedes principle (ASTM C20). After measuring the suspended, saturated, and dried weights of each composite material, the apparent densities were calculated. The relative density of each sample was obtained by calculating the apparent density divided by the theoretical density. In addition, the shrinkage ratios before and after heat treatment were calculated using the dimensional changes.

The as prepared composite materials were polished using diamond paste (subsequently with 6, 3 and 1 μm grains) to observe their microstructures and to introduce cracks.

To introduce cracks into the samples, Vickers indentation was performed by applying a load P of 1.96 and 9.8 N on the polished surface using a hardness tester (HM-114, Mitutoyo, Japan). Vickers indentation was performed on the samples with and without healing treatment.

To heal the cracks of the mullite + Yb_2SiO_5 composite, a sample with a diameter of 25.4 mm was placed in an electric furnace and that was heated in air at a rate of 5 °C/min. The sample was maintained at 1350–1500 °C for 2–10 h, and this cycle was repeated between one and three times. For the crack healing of the mullite + Yb_2SiO_5 composite with Ti_2AlC healing particles, the sample was heated at the same rate of 5 °C/min and maintained at 800–1000 °C for 1 h, and then cooled down to room temperature.

The crystalline phases of the mullite + Yb_2SiO_5 composites with Ti_2AlC healing particles were analyzed using an X-ray diffractometer (RINT-2500HF, Rigaku, Japan) operated with Cu Kα radiation generated at 45 kV.

The healed area and the crack were observed using optical microscopy (Olympus, Japan) and scanning electron microscopy (SEM, JSM-6701F, JEOL, Japan). X-ray micro analysis (XMA) using Energy-dispersive X-ray spectroscopy (EDS) was employed to determine the chemical composition and the element distribution in the healed zones. In addition, scanning electron microscopy combined with a xenon plasma focused ion beam (Helios G4 PFIB UXe, Thermo Fisher Scientific, USA) was performed to create cross-sections to obtain information on the precipitation underneath the free surface.

The strength of each sample was measured before and after healing by the 4-point flexural strength test using a universal testing machine

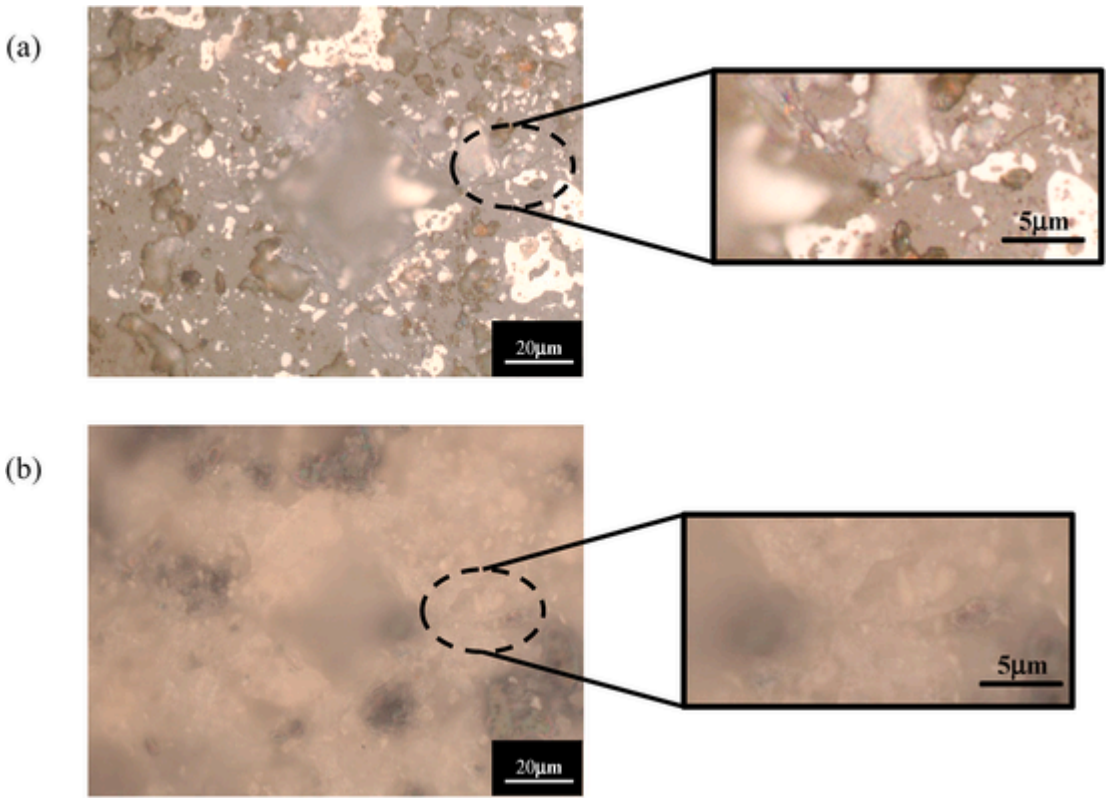

Fig. 6. Optical micrographs of the mullite + Yb_2SiO_5 composite with Ti_2AlC embedded particles: (a) before crack healing and (b) after crack healing in air at 1,000 °C for 2 h. Note that the radial cracks (P = 9.8 N) were healed by oxidation of embedded Ti_2AlC particles.

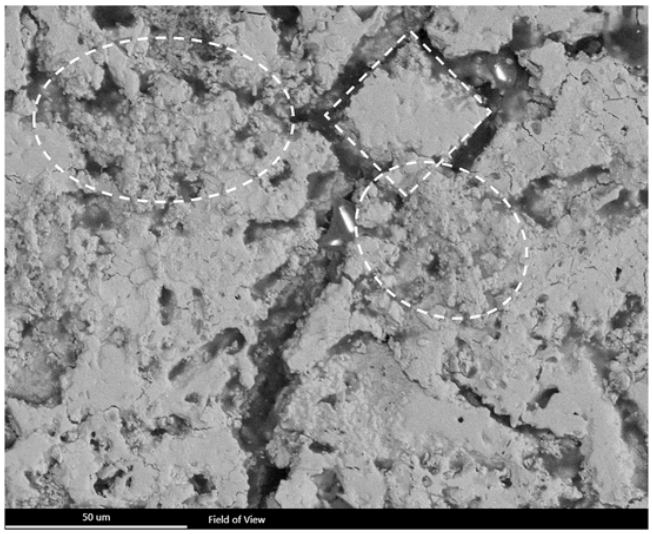

Fig. 7. SEM micrographs of the mullite + Yb_2SiO_5 composite with Ti_2AlC embedded particles healed in air at 1,000 °C for 2 h after removing surface oxides by polishing. The dotted areas correspond to the radial crack area, indicating the occurrence of crack healing.

(Model 5567, Instron Corp., Canton, MA, USA). The 4-point flexural strength test jig has a lower span length of 30 mm and an upper span length of 10 mm. To evaluate the strength recovery after crack healing, the mullite + Yb_2SiO_5 composite with and without Ti_2AlC healing particles were machined to sample sizes of 35 mm × 4 mm × 3 mm. A diamond wheel was used to machine the upper and lower surfaces, and the upper surface was sequentially polished with diamond pastes with 25, 16, 6, 3, and 1 μm grains, respectively. To prevent edge damage, the edges were chamfered using a diamond wheel. Cracks were introduced by Vickers indentation at the center of the samples applying a load P of 9.8 N. To heal the radial cracks, post-heat treatment was conducted at 1350–1500 °C in air for the mullite + Yb_2SiO_5 composite and at 1000 °C in air for the Ti_2AlC-added mullite + Yb_2SiO_5 composite with Ti_2AlC healing particles. Samples both with and without healing particles were placed in the 4-point flexural strength test jig, which was moved downward with a speed of 0.5 mm/min to apply tensile stress on a non-cracked, cracked or healed part.

Furthermore, to infer the mechanical behavior of the composite materials, such as relative hardness and stiffness, the indentation load–displacement curves as obtained during spherical indentation and unloading using a tungsten carbide (WC) sphere with a radius of r = 3.18 mm at a load of P = 0–500 N utilizing the same universal testing instrument. The relative stiffness was analyzed based on the tangential slope of the unloading curve, and the relative hardness was determined by calculating the residual displacement after unloading based on the values before the healing treatment [25,37].

Table 1 summarizes the materials prepared in this study, their basic densities, the hardness and the relative elastic modulus properties of the mullite + Yb_2SiO_5 composite with and without Ti_2AlC healing particles compared with those of mullite. The properties before and after healing of cracks are also compared.

3. Results and discussion

3.1. Crack healing in Mullite-Yb_2SiO_5 EBC material

An example of the cracks introduced into the sintered EBC material by Vickers indentation is shown in Fig. 1. Irreversible damage was caused by the diamond-shaped indentation and radial cracks were generated from each corner. These cracks represent semicircular cracks, as was evident when viewed from the side [45] and are termed radial

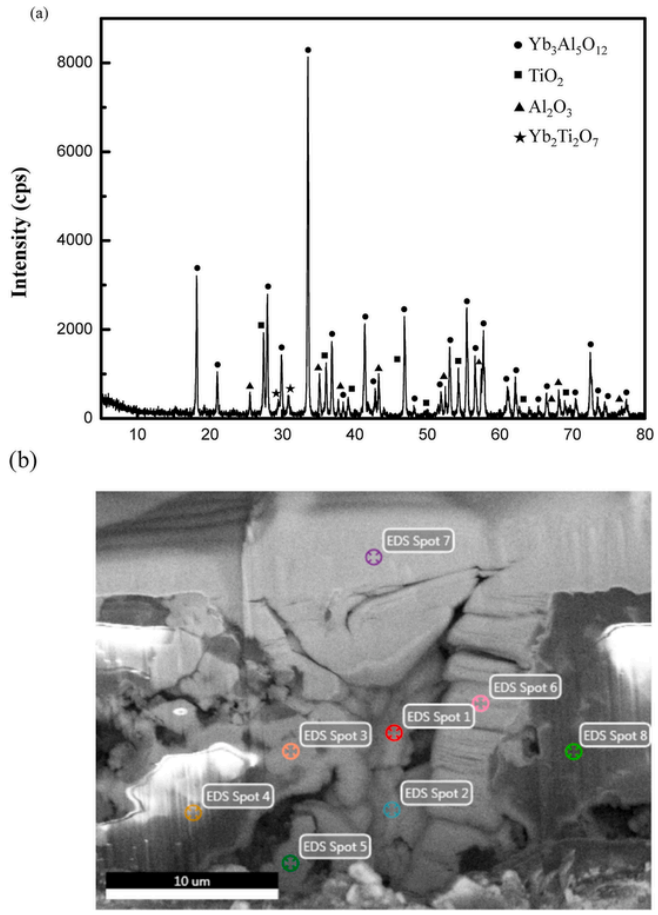

Fig. 8. Analysis of the mullite + Yb_2SiO_5 composite with Ti_2AlC embedded particles after crack healing at 1000 °C in air for 2 h. (a) X-ray diffractogram of the surface oxides, and (b) SEM image of cross section of the crack healed zone as obtained with plasma focused ion beam. The spots indicated in (b) are the locations of chemical composition analysis with EDS; see Table 2. Note that, spots 1 and 2 pertain to the healed crack, spot 7 is located in the Pt deposited layer and the other spots are located in the matrix.

cracks. In this study, the load was controlled such that the length of the radial crack on one side of the indentation was about 15–20 μm.

The cracks introduced by Vickers indentation on the surface of the mullite + Yb_2SiO_5 EBC sample are shown in Fig. 2. The left optical micrograph, Fig. 2a, shows the cracks observed prior to heat treatment for crack healing, and the right optical micrograph, Fig. 2b, depicts the crack site following three cycles of heat treatment at 1350 °C for 10 h. Moreover, Fig. 2b shows that the cracks that advanced in the up and down directions have healed. A sizeable reduction in the length of the radially propagated crack occurred after crack healing. However, since complete healing did not occur in the mullite + Yb_2SiO_5 EBC sample, the temperature was increased to attempt further healing. Fig. 2c and d shows the cracks before and after heat treatment at 1500 °C for 2 h, respectively. As can be seen, most of the radial cracks that developed from irreversible damage have healed after the heat treatment. Furthermore, the formation of a liquid phases at the surface is apparent. Although, the healing of the crack damage at 1500 °C in air is superior to that at 1350 °C, a lower temperature for complete healing is desired. To achieve this, an investigation was conducted in which an additional phase was incorporated into the EBC material, namely Ti_2AlC MAX phase particles; see Section 3.2.

The morphology and composition around the indentation sites of the crack-healed mullite + Yb_2SiO_5 EBC sample at 1500 °C for 2 h was studied using SEM and XMA; see Fig. 3. Fig. 3a includes the diamond-shaped indentation site indicated by a dotted line. The X-ray analysis only detected the elements Yb, Si, O, and Al, and their distribution is shown in Fig. 3 b till e, respectively. The Al map (Fig. 3b) is complementary to the Yb map (Fig. 3c). Considering that the main components of mullite ($3Al_2O_3{\cdot}2SiO_2$) are Al and Si and as Yb_2SiO_5 was added, these maps show also the distribution of both phases in the composite. According to the results of our previous studies [22,37], when the Yb_2SiO_5 phase was added to mullite, XRD analysis detected Al_2O_3 together with mullite, Yb_2SiO_5, and $Yb_2Si_2O_7$. In these studies, the healing mechanism was disclosed: the low-melting-point phase containing SiO_2 migrated into the cracks to fill the crack gaps, while the Al_2O_3 and mullite phases were detected as crystalline phases during cooling. The Al_2O_3 phase is preferred over the SiO_2 phase because of its better resistance against high-temperature corrosion.

3.2. Crack healing in Mullite-Yb_2SiO_5 EBC material by addition of Ti_2AlC

The MAX phase Ti_2AlC synthesized from Ti, TiC, and Al powders at a temperature of 1500 °C, cf. Section 2, is confirmed with XRD; see Fig. 4a. The recorded diffractogram clearly shows that the diffraction lines precisely coincide with the lines pertaining to single phase crystalline Ti_2AlC.

The optical micrograph of the mullite + Yb_2SiO_5 composite with addition of Ti_2AlC particles is shown in Fig. 4b. The matrix material is mullite, the gray phase is Yb_2SiO_5 (some of the Yb_2SiO_5 phase is indicated in the image), and the white area corresponds to the Ti_2AlC MAX phase. The small dark spots are pores. Overall, despite the presence of some agglomerations, the Yb_2SiO_5 and Ti_2AlC phases are distributed

Table 2
Analysis results of chemical compositions on the spot areas near crack healing zone in Fig. 8(b).

El.	spot 1		spot 2		spot 3		spot 4		spot 5		spot 6		spot 7		spot 8	
	wt%	at%	wt%	at%	wt%	at%	wt%	at%	wt%	at%	wt%	at%	wt%	at%	wt%	at%
Yb	67.93	27.5	73.36	42.86	52.64	11.14	1.71	0.2	55.16	12.44	2.44	0.79	1.51	0.31	1.33	0.16
Si	0.65	1.63	0	0	0.79	1.03	0.1	0.08	0.76	1.06	0.17	0.33	0.12	0.15	0.05	0.04
Ti	8.11	11.86	13.52	28.55	1.45	1.11	0.46	0.2	1.86	1.51	2.46	2.85	2.96	2.18	0.49	0.22
Al	2.52	6.53	1.66	6.23	18.67	25.34	51.26	39.38	18.57	26.87	1.43	2.94	1.02	1.32	56.14	44.07
O	6.84	29.95	2.83	17.9	23.78	54.43	46.31	60	22.19	54.16	4.03	14	5.36	11.78	41.92	55.5
C	3.2	18.67	0	0	2.25	6.87	0.07	0.13	1.2	3.91	12.34	57.12	24.85	72.71	0	0

*Pt balanced

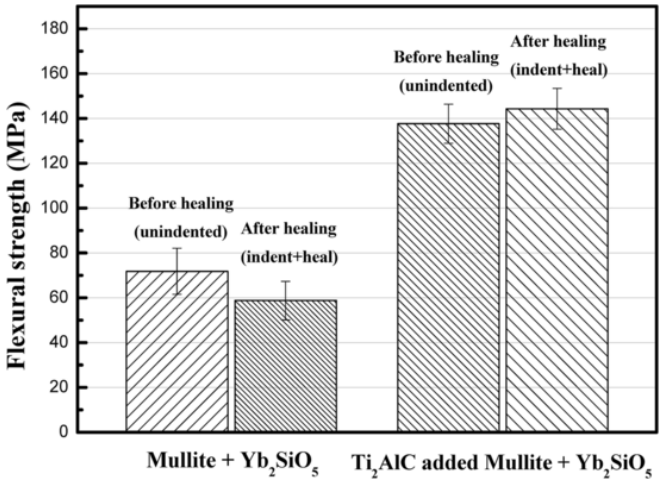

Fig. 9. Flexural strength the mullite + Yb_2SiO_5 composite with and without Ti_2AlC embedded particles of the as prepared material and after crack healing.

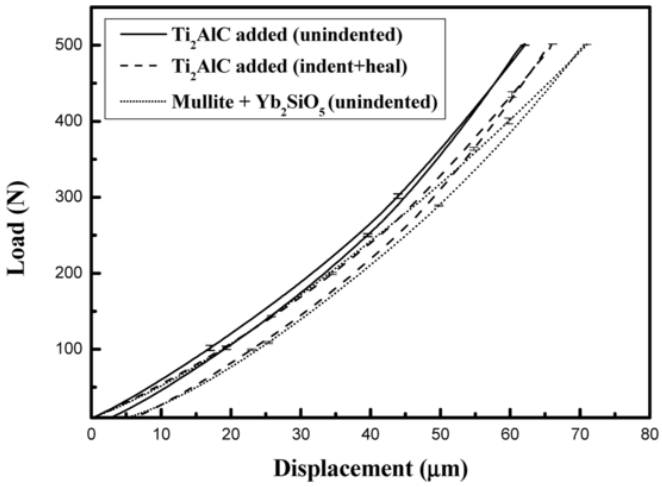

Fig. 10. Indentation load–displacement curves of the mullite + Yb_2SiO_5 composite without healing and the Ti_2AlC-added mullite + Yb_2SiO_5 composite with Ti_2AlC embedded particles before and after crack healing.

uniformly. The distribution of the Ti_2AlC phase, which is the crack-healing agent, appears to be evenly dispersed.

The relative densities of the mullite + Yb_2SiO_5 composite with and without Ti_2AlC MAX phase prepared at the same sintering temperature of 1500 °C are compared in Fig. 5. By adding 20 wt% Ti_2AlC to the mullite + Yb_2SiO_5 mixture the relative density increased from 83.5% to nearly full dense. The higher density of the disc shaped sample was caused by a greater shrinkage due to the addition of Ti_2AlC; the shrinkage ratio was 10.5% in the radial direction and 9.2% in the thickness direction, respectively. A higher density of mullite + Yb_2SiO_5 composite with Ti_2AlC EBC material may be beneficial for protecting the underlying SiC–SiC composite from water vapor penetration.

In the optical micrograph of the mullite + Yb_2SiO_5 composite with Ti_2AlC a radial crack induced by the Vickers indentation is clearly visible; see Fig. 6a. This crack interacts with a Ti_2AlC particle in the mullite + Yb_2SiO_5 composite matrix. The crack damage is healed after subsequent heat treatment at 1000 °C in air; see Fig. 6b.

In the SEM image in Fig. 7, crack healing by the addition of a Ti_2AlC phase is more apparent. The crack-healing mechanism by Ti_2AlC occurs by the oxidation of both Ti and Al, cf. Ref. [46], and the oxides filling the crack gap due to volume expansion upon oxidation. Finally, the strength recovery is due to strong adhesion between the oxides in the crack gap and the parent matrix; see below.

The phases on the surface after heat treatment at 1000 °C in air of the Ti_2AlC MAX phase particles added to the EBC composite were analyzed by XRD; see Fig. 8a. From these findings, it can be conceived the crack healing occurs due to the formation of initially Al_2O_3 and TiO_2 by oxidation of Ti_2AlC. The results of the EDS analysis of the crack healed zone following oxidation are presented in Fig. 8b. The analysis detects both the Al and Ti phases together with the O peak as shown in Table 2. Subsequently these oxides react with Yb_2SiO_5 resulting in the formation of ternary oxides $Yb_3Al_5O_{12}$ and $Yb_2Ti_2O_7$ according to Fig. 8a. According to XRD and XMA, the radial crack is presumably filled with mainly Al_2O_3 and TiO_2 due to oxidation of Ti_2AlC [46]. Also, the surface is covered with oxides stemming from the Ti_2AlC addition. These observations are in agreement with our previous studies on the oxidation of Ti_2AlC MAX phase either as particles [46] or as bulk material [47]. We can expect that the hot corrosion resistance of these oxides are much better than SiO_2 as there is no Si present in the Ti_2AlC particles and then it oxides to Al_2O_3, TiO_2, $Yb_3Al_5O_{12}$ and $Yb_2Ti_2O_7$ [48,49].

The oxidation of Ti_2AlC is a continuous process that occurs not only at a temperature of 1000 °C but also up to 1600 °C [50–52]. Consequently, the gas turbine parts that are targeted for crack healing in this study can expect crack healing by oxidation of Ti_2AlC [48]. During the oxidation test of Ti_2AlC at 1000–1300 °C, reportedly, a α-Al_2O_3 phase forms on the inside and a discontinuous TiO_2 outer layer develops [49]. The oxidation of Ti_2AlC in the range of 1400–1600 °C under a steam atmosphere has also been investigated [48,50]. In addition to the α-Al_2O_3 phase, the Al_2TiO_5 phase is formed on the outer layer; consequently, 1555 °C is suggested to be the highest temperature for applications [50].

The flexural strengths of the mullite + Yb_2SiO_5 EBC and MAX-added EBC samples are presented in Fig. 9. The graph shows the strength of each sample as measured before (un-indented i.e., as prepared material) and after crack healing (indented at $P = 9.8$ N and post-healed material). In the case of the mullite + Yb_2SiO_5 sample, the strength of as prepared material was 71.8 ± 10.3 MPa, while that after crack healing was 58.7 ± 8.6 MPa. This demonstrates a strength recovery of about 82% compared to its initial strength value. Considering that the reduction in strength due to Vickers indentation is about 50% or less of the initial strength [45], this strength recovery is large indicating a significant crack healing effect. The strength of our sample with Vickers-indented without healing was measured at 39.8 ± 6.1 MPa, which is 55% compared to as-prepared material. Conversely, as shown in the graph, the addition of the MAX phase increased the value of the flexural strength from 121 ± 33 MPa before crack healing (i.e. as prepared material) to 144 ± 9 MPa after crack healing, indicating a relatively high strength value following healing.

This all means that the material completely recovered from the loss of strength via the self-healing of cracks after heat treatment of Ti_2AlC at a lower temperature of 1000 °C (>100%). An examination of the origin of the failure following the strength test revealed that the fracture occurred in the vicinity of the indentation site rather than at the indentation site itself, indicating that the crack was completely healed.

From the indentation load–displacement curves of the EBC materials values for the hardness and stiffness (i.e., Young's modules) were obtained; see Fig. 10 and Table 1. The graph comprises the indentation load–displacement of the mullite + Yb_2SiO_5 composite and shows that the indentation load–displacement curves by the addition of Ti_2AlC particles are shifted upward. This indicates that both the hardness and Young's modulus increased by the addition of Ti_2AlC particles, since the hardness is inversely proportional to the amount of residual displacement after unloading and the stiffness is proportional to the slope of the loading or unloading curve. Albeit the curve of the Ti_2AlC-added mullite + Yb_2SiO_5 composite is slightly shifted downward after crack healing due to the formation of oxides (see the graph designated by

'Ti_2AlC added (indented + heal)'), the mechanical properties remain superior to that of the mullite + Yb_2SiO_5 composite without the addition of Ti_2AlC, cf. Fig. 10 and Table 1.

4. Conclusions

The crack healing capacity of mullite + Yb_2SiO_5 composite with and without embedded Ti_2AlC MAX phase particles was investigated. The mullite + Yb_2SiO_5 material is used as environmental barrier coating (EBC) on SiC–SiC ceramic matrix composites (CMC) for critical high temperature applications, such as components in jet engines for aircrafts and spacecrafts.

The healing of cracks in the mullite + Yb_2SiO_5 EBC material without Ti_2AlC required a heat treatment at very high temperatures, i.e., 1300 °C or 1500 °C for 2–30 h. Then, the cracks were filled by a eutectic liquid phase containing SiO_2 resulting in an ~80% strength recovery.

On the other hand, full crack healing was realized in the mullite + Yb_2SiO_5 composite with embedded Ti_2AlC MAX phase particles at significant lower temperatures and within shorter times; e.g., 1000 °C for 2 h. The cracks were filled with Al_2O_3 and TiO_2. Subsequently, these oxidation products react with the composite matrix forming ternary oxides like $Yb_2Ti_2O_7$ and $Yb_3Al_5O_{12}$. These ternary oxides also formed on the surface to completely conceal the cracks.

Finally, the embedded Ti_2AlC enhanced the hardness and stiffness of the mullite + Yb_2SiO_5 composite as well as the strength with full strength recovery after crack healing.

Declaration of competing interest

The authors declare that they have no known competing financial interests or personal relationships that could have appeared to influence the work reported in this paper.

Acknowledgements

This study was supported by the IT R&D program of MOTIE/KEIT [NO. 20000192, Development on the crack self-healing technology of CMC composite and coating material for gas turbine hot gas component]. The authors also wish to thank Mr. Soo Min Park and Dr. Sung Min Lee for experimental analysis.

References

[1] R.S. Lima, D. Zhu, L. Li, Thermal and environmental barrier coatings (TBCs/EBCs) for turbine engines, Handb. Therm. Spray. Technol. 5A (2013) 270–279.
[2] J.C. Zhao, J.H. Westbrook, Ultrahigh-temperature materials for jet engines, MRS Bull. 28 (2003) 622–630.
[3] J. Kulczyk-Malecka, X. Zhang, J. Carr, F. Nozahic, C. Estournès, D. Monceau, A.L. Carabat, W.G. Sloof, S. van der Zwaag, P.J. Withers, P. Xiao, Thermo – mechanical properties of SPS produced self-healing thermal barrier coatings containing pure and alloyed $MoSi_2$ particles, J. Eur. Ceram. Soc. 38 (12) (2018) 4268–4275.
[4] F. Nozahic, C. Estournès, A.L. Carabat, W.G. Sloof, S. van der Zwaag, D. Monceau, Self-healing thermal barrier coating systems fabricated by spark plasma sintering, Mater. Des. 143 (2018) 204–213.
[5] M.O. Jarligo, T. Steinke, D.E. Mack, D. Stöver, R. Vaβen, Overview on advanced thermal barrier coatings, Surf. Coating. Technol. 205 (2010) 938–942.
[6] B.K. Jang, N. Nagashima, S. Kim, Y.-S. Oh, S.-M. Lee, Mechanical properties and microstructure of Yb_2SiO_5 environmental barrier coatings under isothermal heat treatment, J. Eur. Ceram. Soc. 40 (2020) 2667–2673.
[7] F.W. Zok, Ceramic-matrix composites enable revolutionary gains in turbine engine efficiency, Am. Ceram. Soc. Bull. 95 (2016) 22–28.
[8] J.L. Smialek, R.C. Robinson, E.J. Opila, D.S. Fox, N.S. Jacobson, SiC and Si_3N_4 recession due to SiO_2 scale volatility under combustor conditions, Adv. Compos. Mater. 8 (1999) 33–45.
[9] K.N. Lee, Current status of environmental barrier coatings for Si-based ceramics, Surf. Coating. Technol. 133–134 (2000) 1–7.
[10] B.J. Harder, K.T. Faber, Transformation kinetics in plasma-sprayed barium- and strontium-doped aluminosilicate (BSAS), Scripta Mater. 62 (2010) 282–285.
[11] J. Kimmel, N. Miriyala, J. Price, K. More, P. Tortorelli, H. Eaton, G. Linsey, E. Sun, Evaluation of CFCC liners with EBC after field testing in a gas turbine, J. Eur. Ceram. Soc. 22 (2002) 2769–2775.
[12] B.-K. Jang, F.J. Feng, K.S. Lee, E. Garcia, A. Nistal, N. Nagashima, S. Kim, Y.-S. Oh, H.-T. Kim, Thermal behavior and mechanical properties of Y_2SiO_5 environmental barrier coatings after isothermal heat treatment, Surf. Coating. Technol. 308 (2016) 24–30.
[13] Z. Tian, L. Zheng, Z. Li, J. Li, J. Wang, Exploration of the low thermal conductivities of γ-$Y_2Si_2O_7$, β-$Y_2Si_2O_7$, β-$Yb_2Si_2O_7$, and β-$Lu_2Si_2O_7$ as novel environmental barrier coating candidates, J. Eur. Ceram. Soc. 36 (2016) 2813–2823.
[14] N.L. Ahlborg, D. Zhu, Calcium-magnesium aluminosilicate (CMAS) reactions and degradation mechanisms of advanced environmental barrier coatings, Surf. Coating. Technol. 237 (2013) 79–87.
[15] S. Ueno, T. Ohji, H.-T. Lin, Recession behavior of Lu_2SiO_5 under a high speed steam jet at high temperatures, Ceram. Int. 37 (2011) 1185–1189.
[16] K.N. Lee, R.A. Miller, Development and environmental durability of mullite and mullite/YSZ dual layer coatings for SiC and Si_3N_4 ceramics, Surf. Coating. Technol. 86–87 (1996) 142–148.
[17] G.D. Girolamo, C. Blasi, L. Pilloni, M. Schioppa, Microstructure and thermal properties of plasma sprayed mullite coatings, Ceram. Int. 36 (2010) 1389–1395.
[18] J.M. Guimarães, E. García, P. Miranzo, M.I. Osendi, C.V. Cojocaru, R.S. Lima, Mullite-YSZ multilayered environmental barrier coatings tested in cycling conditions under water vapor atmosphere, Surf. Coating. Technol. 209 (2012) 103–109.
[19] E. Bakan, M. Kindelmann, W. Kunz, H. Klemm, Rober Vaβen, High-velocity water vapor corrosion of Yb-silicate: sprayed vs. sintered body, Scripta Mater. 178 (2020) 468–471.
[20] E. Garcia, H. Lee, S. Sampath, Phase and microstructure evolution in plasma sprayed $Yb_2Si_2O_7$ coatings, J. Eur. Ceram. Soc. 39 (2019) 1477–1486.
[21] D.L. Poerschke, J.S.V. Sluytman, K.B. Wong, C.G. Levi, Thermochemical compatibility of ytterbia-(hafnia/silica) multilayers for environmental barrier coatings, Acta Mater. 61 (2013) 6743–6755.
[22] F.J. Feng, B.-K. Jang, J.Y. Park, K.S. Lee, Effect of Yb_2SiO_5 addition on the physical and mechanical properties of sintered Mullite ceramic as an environmental barrier coating material, Ceram. Int. 42 (2016) 15203–15208.
[23] B.-K. Jang, F.-J. Feng, K. Suzuta, H. Tanaka, Y. Matsushita, K.S. Lee, S. Ueno, Corrosion behavior of volcanic ash and calcium magnesium aluminosilicate on Yb_2SiO_5 environmental barrier coatings, J. Ceram. Soc. Jpn. 125 (2017) 326–332.
[24] X. Zhang, C. Wang, R. Ye, C. Deng, X. Liang, Z. Deng, S. Niu, J. Song, G. Liu, M. Liu, K. Zhou, J. Lu, J. Feng, Mechanism of vertical crack formation in Yb_2SiO_5 coatings deposited via plasma-physical vapor deposition, J. Materiomics 6 (2020) 102–108.
[25] D.H. Lee, K.S. Lee, T.W. Kim, C. Kim, Hertzian stress analysis and characterization of thermal barrier coatings containing unidirectional vertical cracks, Ceram. Int. 45 (2019) 21348–21358.
[26] A. Jadhav, N.P. Padture, F. Wu, E.H. Jordan, M. Gell, Thick ceramic thermal barrier coatings with high durability deposited using solution-precursor plasma spray, Mater. Sci. Eng. 405 (2005) 313–320.
[27] B.T. Richards, S. Sehr, F. Franqueville, M.R. Begley, H.N.G. Wadley, Fracture mechanisms of ytterbium monosilicate environmental barrier coatings during cyclic thermal exposure, Acta Mater. 103 (2016) 448–460.
[28] A.G. Evans, J.W. Hutchinson, The mechanics of coating delamination in thermal gradient, Surf. Coating. Technol. 201 (2007) 7905–7916.
[29] J. Kulczyk-Malecka, X. Zhang, J. Carr, A.L. Carabat, W.G. Sloof, S. van der Zwaag, F. Cernuschi, F. Nozahic, D. Monceau, C. Estournes, P.J. Withers, P. Xiao, Influence of embedded $MoSi_2$ particles on the high temperature thermal conductivity of SPS produced yttria-stabilised zirconia model thermal barrier coatings, Surf. Coating. Technol. 308 (2016) 31–39.
[30] P. Greil, Generic principles of crack-healing ceramics, J. Adv. Ceram. 1 (2012) 249–267.
[31] K. Ando, K. Furusawa, K. Takahashi, S. Sato, Crack-healing ability of structural ceramics and a new methodology to guarantee the structural integrity using the ability and proof-test, J. Eur. Ceram. Soc. 25 (2005) 549–558.
[32] S. Li, L. Xiao, G. Song, X. Wu, W.G. Sloof, S. van der Zwaag, Oxidation and crack healing behavior of a fine-grained Cr_2AlC ceramic, J. Am. Ceram. Soc. 96 (2013) 892–899.
[33] L. Boatemaa, S. van der Zwaag, W.G. Sloof, Self-healing of Al_2O_3 containing Ti microparticles, Ceram. Int. 44 (2018) 11116–11126.
[34] W.G. Sloof, A. S, L. Shen, Intrinsic autonomous crack healing in MAX phase ceramics, in: S. van der Zwaag, E. Brinkman (Eds.), Self Healing Materials - Pioneering Research in the Netherlands, IOS Press, Amsterdam, 2015, pp. 113–118.
[35] S.K. Lee, W. Ishida, S.-Y. Lee, K.-W. Nam, K. Ando, Crack-healing behavior and resultant strength properties of silicon carbide ceramic, J. Eur. Ceram. Soc. 25 (2005) 569–576.
[36] K.W. Nam, J.S. Kim, Critical crack size of healing possibility of SiC ceramics, Mater. Sci. Eng. 527 (2010) 3236–3239.
[37] H.-I. Seo, D. Kim, K.S. Lee, Crack healing in mullite-based EBC during thermal shock cycle, Coatings 9 (2019) 585, https://doi.org/10.3390/coatings9090585.
[38] A.-S. Farle, C. Kwakernaak, S. van der Zwaag, W.G. Sloof, A conceptual

study into the potential of $M_{n+1}AX_n$-phase ceramics for self-healing of crack damage, J. Eur. Ceram. Soc. 35 (2015) 37–45.
[39] M. Radovic, M.W. Barsoum, MAX phases: bridging the gap between metals and ceramics, Am. Ceram. Soc. Bull. 92 (2013) 20–27.
[40] L. Boatemaa, C. Kwakernaak, S. van der Zwaag, W.G. Sloof, Selection of healing agents for autonomous healing of alumina at high temperatures, J. Eur. Ceram. Soc. 36 (2016) 4141–4145.
[41] A.S. Farle, C. Kwakernaak, S. van der Zwaag, W.G. Sloof, A conceptual study into the potential of $M_{n+1}AX_n$-phase ceramics for self-healing of crack damage, J. Eur. Ceram. Soc. 35 (1) (2015) 37–45.
[42] S.B. Li, G.M. Song, K. Kwakernaak, S. van der Zwaag, W.G. Sloof, Multiple crack healing of a Ti_2AlC ceramic, J. Eur. Ceram. Soc. 32 (8) (2012) 1813–1820.
[43] W.G. Sloof, R. Pei, S.A. McDonald, J.L. Fife, L. Shen, L. Boatemaa, A.S. Farle, K. Yan, X. Zhang, S. van der Zwaag, P.D. Lee, P.J. Withers, Repeated crack healing in MAX-phase ceramics revealed by 4D in situ synchrotron X-ray tomographic microscopy, Sci. Rep. 6 (2016) 23040.
[44] T. Osada, A. Watabe, J. Yamamoto, J.C. Brouwer, C. Kwakernaak, S. Ozaki, S. van der Zwaag, W.G. Sloof, Full strength and toughness recovery after repeated cracking and healing in bone-like high temperature ceramics, Sci. Rep. 10 (1) (2020) 18990.
[45] B.R. Lawn, Fracture of Brittle Solids, in: E.A. Davis, I.M. Ward FRS(Eds.) Cambridge University Press, New York, pp. 264-276.
[46] L. Boatemaa, M. Bosch, A.S. Farle, G.P. Bei, S. van der Zwaag, W.G. Sloof, Autonomous high-temperature healing of surface cracks in Al_2O_3 containing Ti_2AlC particles, J. Am. Ceram. Soc. 101 (2018) 5684–5693.
[47] G.M. Song, V. Schnabel, C. Kwakernaak, S. Van der Zwaag, J.M. Schneider, W.G. Sloof, High temperature oxidation behaviour of Ti_2AlC ceramic at 1200°C, Mater. A. T. High. Temp. 29 (3) (2012) 205–209.
[48] Z.J. Lin, M.S. Li, J.Y. Wang, Y.C. Zhou, Influence of water vapor on the oxidation behavior of Ti_3AlC_2 and Ti_2AlC, Scripta Mater. 58 (2008) 29–32.
[49] E.J. Opila, D.L. Myers, Alumina volatility in water vapor at elevated temperatures, J. Am. Ceram. Soc. 87 (9) (2004) 1701–1705.
[50] M. Haftani, M.S. Heydari, H.R. Baharvandi, N. Ehsani, Studying the oxidation of Ti_2AlC MAX phase in atmosphere: a review, Int. J. Refract. Metals Hard Mater. 61 (2016) 51–60.
[51] X.H. Wang, Y.C. Zhou, High-temperature oxidation behavior of Ti_2AlC in air, Oxid. Metals 59 (2003) 303–320.
[52] C. Tang, M. Steinbruck, e Mirco Bro, T. Bergfeldt, H.J. Seiert, Oxidation behavior of Ti_2AlC in the temperature range of 1400°C-1600°C in steam, J. Nucl. Mater. 490 (2017) 130–142.